Journal of Power Sources 194 (2009) 31–37

Contents lists available at ScienceDirect

Journal of Power Sources

journal homepage: www.elsevier.com/locate/jpowsour

Electrochemical impedance spectroscopy of $BaCeO_3$ modified by Ti and Y

P. Pasierb*, M. Wierzbicka, S. Komornicki, M. Rekas

AGH University of Science and Technology, Faculty of Materials Science and Ceramics, Al. Mickiewicza 30, 30-059 Krakow, Poland

ARTICLE INFO

Article history:
Received 18 October 2008
Received in revised form 28 January 2009
Accepted 29 January 2009
Available online 12 February 2009

Keywords:
Protonic conductors
Barium cerium oxide
Electrochemical impedance spectroscopy

ABSTRACT

Barium cerate exhibits high protonic conductivity, especially when modified by trivalent dopant such as Y, Yb, Nd, Sm or Dy. Unfortunately, the poor chemical stability in the presence of CO_2 is the main disadvantage of this material. One of the possible approach to get the stable protonic conductor is the preparation of solid solutions. For example, doping of $BaCeO_3$ with Zr leads to the improvement of the chemical stability, but the electrical properties are simultaneously corrupted.

In the present work the influence of Ti, per analogy to Zr, and Y dopants on electrical properties of $BaCeO_3$ was investigated using the electrochemical impedance spectroscopy (EIS) technique. $BaCe_{1-x}Ti_xO_{3-\delta}$ $(0 \le x \le 0.3)$ and $Ba(Ce_{0.95}Ti_{0.05})_{0.95}Y_{0.05}O_{3-\delta}$ solid electrolytes were prepared by solid-state reaction method. It was found that the changes of electrical properties due to the introduction of Ti into the $BaCeO_3$ lattice is caused predominantly by the modification of the grain boundary properties. The Ti doping leads to the substantial decrease of grain boundary electrical conductivity, comparing to undoped material. The introduction of yttrium dopant to the $BaCe_{0.95}Ti_{0.05}O_3$ lattice has the opposite effect. The total electrical conductivity increases, due to significant modification of grain boundary electrical properties.

1. Introduction

The results indicating a considerable proton conduction under hydrogen-containing atmosphere at elevated temperatures in $SrCeO_3$- and $BaCeO_3$-based perovskite-type oxides were published during last 25 years, e.g. [1,2]. These materials may be used as electrolytes in solid oxide fuel cells (SOFC), membranes for hydrogen purification, membrane reactors for different organic syntheses or in gas sensors, e.g. [3]. Undoped $BaCeO_3$ at oxygen-rich gas atmosphere (e.g. in both dry or wet air) exhibits low p-type electronic conductivity [4,5]. No significant differences of electrical conductivity was observed in dry and wet air [6]. When oxygen partial pressure decreases, the p- to n-type transition is observed [6,7]. Such behavior can be explained in terms of oxygen nonstoichiometry and intrinsic electronic disorder:

$$O_O \Leftrightarrow V_O^{\bullet\bullet} + 2e' + \frac{1}{2}O_{2(g)} \quad (1)$$

$$\text{nill} \Leftrightarrow e' + h^{\bullet} \quad (2)$$

Decrease of oxygen partial pressure is commonly realized by the use H_2/H_2O gas mixtures. Replacement of air by H_2 gas atmosphere leads to considerable increase of total electrical conductivity of $BaCeO_3$ (about 10-times), its activation energy changes from ca. 1.8 eV to 0.62 eV [6]. Detailed analysis revealed that then protonic conductivity component assumes high values [8]. The effect of gas atmosphere change from air to hydrogen over $BaCeO_3$ has complex meaning.

First, according to Eq. (1) predominant in air electron holes are replaced by electrons (n-type electronic conductivity). Taking into considerations large differences in mobilities and activation energies of electron and holes conductivity in $BaCeO_3$ and its closed analog $SrCeO_3$ determined by Bonanos [9] and Kosacki and Tuller [7] the p- to n-transition may have the strong effect on total electrical conductivity.

Second, protonic defects form according to the reaction:

$$H_{2(g)} + V_O^{\bullet\bullet} + 2O_O^x \Leftrightarrow 2(OH)_O^{\bullet} \quad (3)$$

Third, changes of cerium valence has been postulated [10]:

$$Ce_{Ce}^x \Leftrightarrow Ce'_{Ce} + h^{\bullet} \quad (4)$$

According to the $BaCeO_3$ formula the valence of cerium is +4, however, in reduction conditions the Ce^{4+} ions (Ce_{Ce}^x in point defect notation) easily reduce to Ce^{3+} (Ce'_{Ce}). As it results from Eq. (3) the presence of oxygen vacancies in the solid promotes formation of protonic defects. High concentration of oxygen vacancies even at oxygen-rich gas atmospheres (e.g. air) may be obtained by acceptor doping of $BaCeO_3$. Several dopants such as Yb_2O_3 [1,2,7], Gd_2O_3 [11], Nd_2O_3 [12–14], Y_2O_3 [6,13,15] and other have been used.

* Corresponding author. Tel.: +48 12 617 25 33; fax: +48 12 617 24 93.
E-mail address: ppasierb@agh.edu.pl (P. Pasierb).

0378-7753/$ – see front matter © 2009 Elsevier B.V. All rights reserved.
doi:10.1016/j.jpowsour.2009.01.098

Denoting cation of dopant by M^{3+} the reaction of M_2O_3 incorporation into $BaCeO_3$ lattice may be written as

$$M_2O_3 + 2BaO \Rightarrow 2Ba_{Ba} + 2M'_{Ce} + V_O^{\bullet\bullet} + 5O_O \quad (5)$$

In the presence of water vapor the creation of protonic defects occurs according to the following reaction:

$$H_2O_{(g)} + V_O^{\bullet\bullet} + O_O^x \Leftrightarrow 2(OH)_O^{\bullet} \quad (6)$$

More detailed, quantitative description of defect structure and related electrical properties of either $BaCeO_3$- or $SrCeO_3$-based materials can be found in Refs. [7,16–19].

The effect of cation ratio Ba/Ce on electrical conductivity is discussed in Refs. [6,20].

The poor chemical stability of $BaCeO_3$ materials, especially in the presence of CO_2 is one of the disadvantages of these materials. Prolonged exposure to CO_2-containing atmospheres leads to the deterioration of mechanical properties of material, due to the formation of secondary barium carbonate and cerium oxide [21,22]. The formation of solid solutions with chemically stable, isostructural $BaZrO_3$ is the successful approach to the improvement of corrosion resistance against the CO_2. Unfortunately, the introduction of Zr leads to the drastic decrease of electrical properties of the material [18]. Recent reports show that simultaneous doping of $BaCeO_3$ by Zr and Nd leads to the material with good chemical stability and increased electrical conductivity [23].

The application of $BaCeO_3$-based protonic conductors will be possible if the electrical conductivity is increased and the chemical stability, especially in gas atmospheres containing CO_2, is improved. Our previous works [8,24] have shown that introduction of titanium into $BaCeO_3$ led to the improvement of chemical stability in the presence of CO_2, but the total DC electrical conductivity decreased by ca. one order of magnitude comparing to the undoped material. Moreover, the transport properties were modified; the introduction of titanium led to the decrease of protonic and the increase of electronic transference numbers in the materials. These results are similar to that observed for Zr-substituted $BaCeO_3$, as mentioned above.

The purpose of this work was to investigate the influence of Ti and Y dopants on the electrical properties of $BaCeO_3$ materials, with the emphasis on the bulk and grain boundary properties analysis. Also, the effect of simultaneous doping by Ti and Y on electrical properties of $BaCeO_3$ was investigated. The adequate for such purpose electrochemical impedance spectroscopy (EIS) technique was used in this work as an experimental tool.

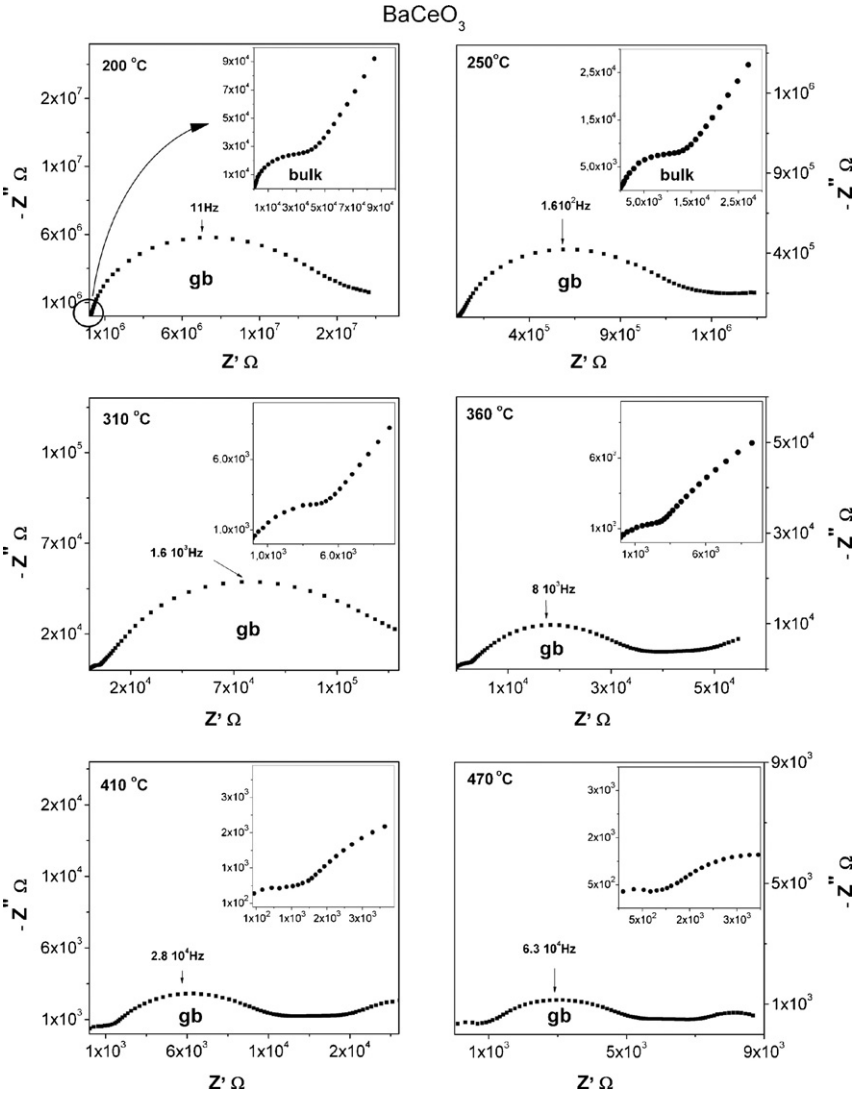

Fig. 1. Example EIS spectra measured for undoped $BaCeO_3$ at different temperatures in H_2–Ar atmosphere (7% H_2 in Ar).

2. Experimental

Powders of $BaCe_{1-x}Ti_xO_{3-\delta}$ ($0 \le x \le 0.3$) and $Ba(Ce_{0.95}Ti_{0.05})_{(1-y)}Y_yO_{3-\delta}$ ($y = 0.05, 0.1, 0.2$) solid electrolytes were prepared by solid-state reaction method. The proper amounts of high-purity starting materials: barium carbonate $BaCO_3$ (99.9%), cerium(IV) oxide CeO_2 (99.9%), TiO_2 nanopowder (99.7%) and water solution of $Y(NO_3)_3$, all reagents supplied by Aldrich Chemical Company, Inc., were used as starting materials. After mixing the starting powders, and the impregnation by required amount of yttrium nitrate solution the materials were calcinated at 1200 °C for 24 h. The obtained materials were crushed, milled in the absolute alcohol suspension using "Pulverisette 6" (Fritsch) mill and ZrO_2 grinding media, formed in a pellet-die (at 25 MPa) and isostatically pressed at 250 MPa. The bodies were sintered in air at 1500 °C for 24 h, then cut using diamond saw and polished to the required shape (rectangular plates 10 mm × 10 mm × 1.8 mm). Prior to the electrical measurements the Pt electrodes ($\phi = 5$ mm) were screen-printed (Demertron Pt paste) from both sides of the plates and fired at 850 °C for 5 min. Prepared samples were stored in the dessicator to avoid any secondary reactions with CO_2 and water vapor.

Electrochemical impedance measurements (EIS) were done using the Solartron FRA1260 coupled with Solartron 1296 Dielectric Interface in a typical sample holder and controlled temperature (200–800 °C) and hydrogen-rich (7% H_2 in Ar) gas atmosphere. Impedance spectra were fitted using Corware Zplot 2.0 software. The experimental data were presented either as Nyquist plots (imaginary part ($-Z''$) *vs.* real part (Z')) or using ρ' and $-\rho''$ parameters *vs.* frequency, where ρ' and $-\rho''$ are defined as real (ρ') and imaginary part ($-\rho''$) of the impedance normalized by the geometrical dimensions of each sample. The geometrical parameter k is equal to $k = A/d$, where A is the area and d is the thickness of sample.

3. Results and discussion

Basing on the XRD results presented previously [8] it can be stated that undoped sample ($x = 0, y = 0$) crystallized in orthorhombic *Pmcn* structure, while the incorporation of titanium into the lattice lead to a gradual ordering of the structure, which was observed as a disappearance of the reflex splitting with the increase of Ti concentration. Also, the shift of reflex maxima towards higher values of 2θ with the increase of Ti was observed, caused by the decrease of lattice constants. The determined solubility limit for Ti in $BaCeO_3$ was found to be between 20 at.% and 30 at.% of Ti. In case of yttrium doped samples with constant Ti concentration ($x = 0.05$) it was observed that the structure gradually changes from tetragonal to regular form with increasing content of yttrium, and no additional phases were detected up to $y = 0.20$ [24].

The scanning electron microscopy measurements [8] indicated almost no influence of Ti concentration on the microstructure of sintered bodies. In all cases dense materials with some apparent porosity were obtained with average grain size of several micrometers.

In this paper the influence of Ti and Y dopants on electrical properties determined using electrochemical impedance spectroscopy is presented. The emphasis is focused on the separation of grain boundary and bulk properties and the effect of titanium and yttrium dopants on the modification of electrical properties of materials.

Fig. 1 shows an example impedance spectra measured for undoped $BaCeO_3$ at different temperatures in H_2–Ar atmosphere. In this case, the separation of high-frequency region corresponding to the bulk properties and an intermediate-frequency region, corresponding to the grain boundary properties can be distinguished for all presented temperatures. Two arcs are visible with clearly higher diameter of arc corresponding to grain boundary, which indicates the blocking properties of grain boundaries. At higher temperatures, above 500 °C, the arc in the high frequency region, corresponding to bulk was not observable.

The presented impedance spectra may be approximated using the equivalent circuit consisting of two serials R and CPE (constant phase element) connected in parallel. Additionally, the electrode resistance $R_{electrode}$ and inductance L of electrical wires connected in parallel may be also considered during the fitting of impedance spectra. The sets of R and CPE elements connected in series correspond to the grain boundary (R_{gb} and CPE_{gb}) and bulk (R_b and CPE_b) properties and were determined separately, where possible.

Fig. 2 shows the dependence of electrical conductivity as a function of temperature, in $\log(\sigma T)$ *vs.* $1/T$ coordinates, determined for grain boundary and bulk from the results as presented in Fig. 1. The total resistances were calculated as $R_{total} = R_b + R_{gb}$ (bulk and grain boundary, respectively). The activation energies of the electrical conductivity were calculated and the strong disproportion in the values obtained for grain boundaries and bulk conductivities was determined. In case of bulk conductivity a discontinuity between 630 K and 740 K is observed. This fact may be interpreted by a phase transition occurring in $BaCeO_3$ at ca. 770 K [25]. The activation energies were equal to 0.089 ± 0.037 eV and 0.433 ± 0.020 eV, at high and low temperatures, respectively. No discontinuity of the grain boundary conductivity is observed and the activation energy was found to be as high as $E_{act(gb)} = 0.931 \pm 0.030$ eV. The obtained results are in agreement with the data presented in literature [26] and follow the general dependence observed for most of the perovskite-type compounds: $E_{act(gb)} \gg E_{act(b)}$. Additionally, the results presented in Fig. 2 indicate that grain boundary properties dominate the overall electrical conductivity at lower temperatures, while at higher temperatures the difference in bulk and grain boundary conductivities becomes insignificant. Presented in Fig. 2 the total electrical conductivity exhibits also some discontinuity (smaller than that of the bulk). Its activation energies are 0.614 ± 0.055 eV and 1.042 ± 0.025 eV at high and low temperatures, respectively. The activation energy 0.614 eV remains in excellent agreement with those determined from the results reported by Ma et al. [6] at similar conditions (temperature range and gas atmosphere): $E_{act,\ total} = 0.615$ eV.

Different situation is observed in case of Ti-doped $BaCeO_3$ samples. Fig. 3A–C shows the example impedance spectra measured for low temperatures (up to 400 °C, for $x = 0.2$; Fig. 3A) and higher temperatures (500 °C and above, for $x = 0.05$; Fig. 3B and $x = 0.2$; Fig. 3C).

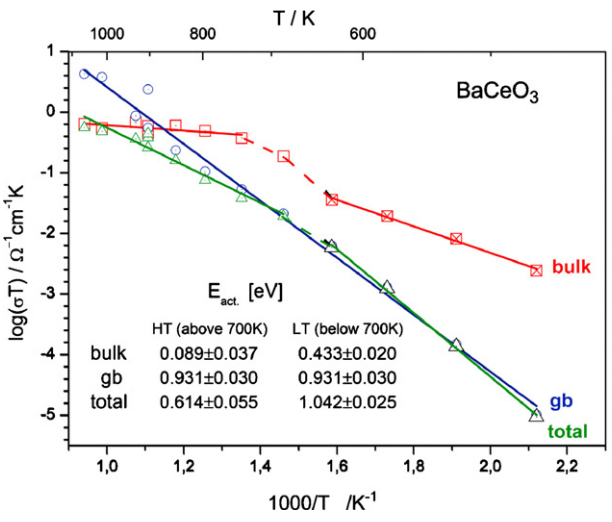

Fig. 2. The dependence of bulk, grain boundary and total electrical conductivity as a function of temperature for undoped $BaTiO_3$, in $\log(\sigma T)$ *vs.* $1/T$ coordinates.

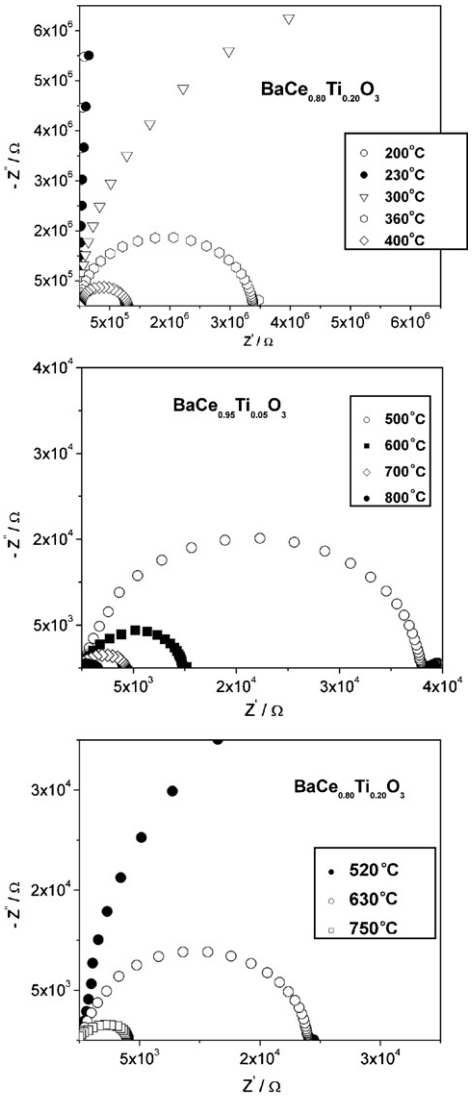

Fig. 3. Example EIS spectra of Ti-doped $BaCeO_3$: at low temperatures, below 400 °C) for $x = 0.2$ (upper graph), at high temperatures (above 500 °C) for $x = 0.05$ (middle graph), and at high temperatures (above 500 °C) for $x = 0.2$ (lower graph).

In all cases only one arc was observed for all compositions, even at temperatures as low as 300 °C. According to the data presented in Fig. 4, where the dependences of $-\rho''$ on frequency for $T = 300$ °C are shown for undoped and Ti ($x = 0.20$) doped $BaCeO_3$, the disappearance of second arc in spectrum can be explained by extremely high blocking properties of grain boundaries caused by Ti doping. In case of undoped $BaCeO_3$ sample two maxima can be observed at $f_{gb} = 1.4 \times 10^3$ Hz and $f_b = 1.4 \times 10^6$ Hz, which are typical frequencies for grain boundary and bulk properties, respectively. In contrary, in case of Ti-doped $BaCeO_3$ sample ($x = 0.20$) only one maximum can be observed at $f_{gb} = 710$ Hz, which can be only associated to grain boundary properties.

Further analysis of the EIS spectra allowed to determine the constant phase element (CPE) parameters. It was found that in the case of undoped sample the CPE-p parameter is in the range of 0.6–0.7 (close to the Wartburg element; 0.5), while CPE-t is in order of 10^{-8} to 10^{-9}. In the case of Ti-doped samples the CPE-p was found to be close to 1 (Debye capacitor), while CPE-t was about 10^{-11}. The proper and unequivocal interpretation of our results and determination of capacitance in the case where the CPE element was involved is not possible. Proposed in literature approaches are different (at selected frequency where the CPE element can be treated as Debye element or, determination of capacitance from the peak frequency) and there is no method to evaluate which is the proper one. So, the discussed in our paper the "CPE-t" parameter is not strictly the capacitance. According to the literature data [27,28] reporting the influence of Ce dopant on the dielectric properties of $BaTiO_3$, where the decrease of permittivity, ε, with the increas-

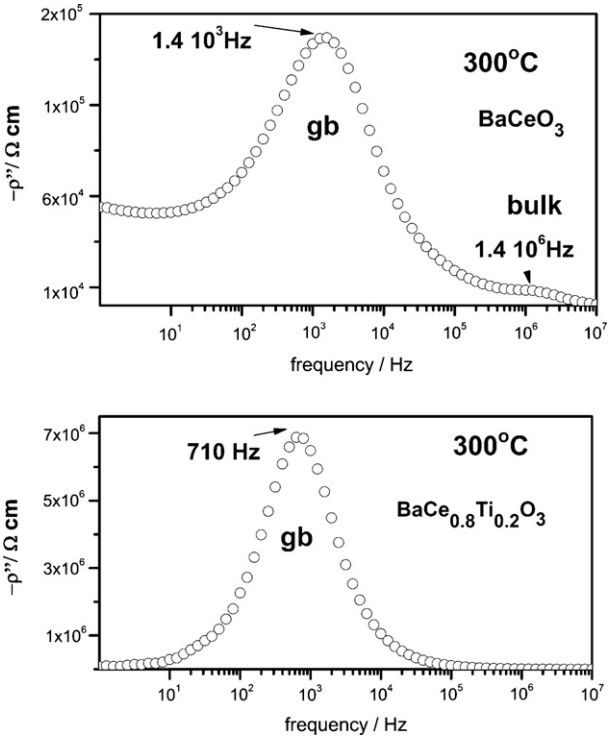

Fig. 4. The comparison of the $-\rho''$ *vs.* frequency for undoped and Ti ($x = 0.20$) doped $BaCeO_3$, for $T = 300$ °C.

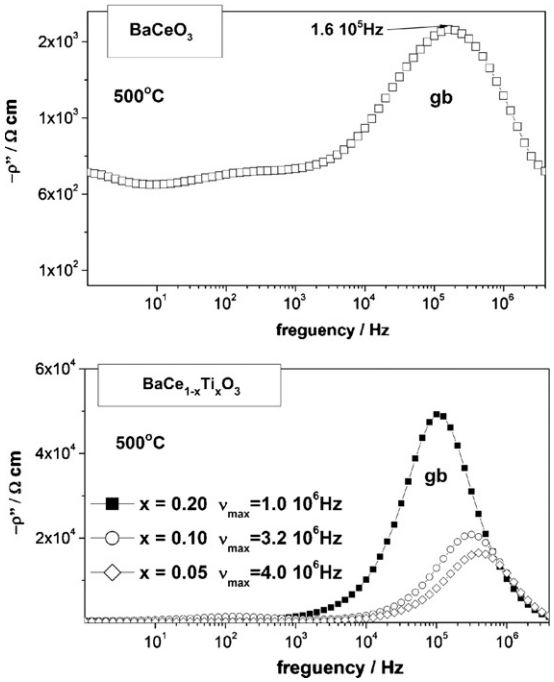

Fig. 5. The comparison of $-\rho''$ *vs.* frequency dependences for undoped and Ti-doped $BaCeO_3$ with different Ti concentrations, for $T = 500$ °C.

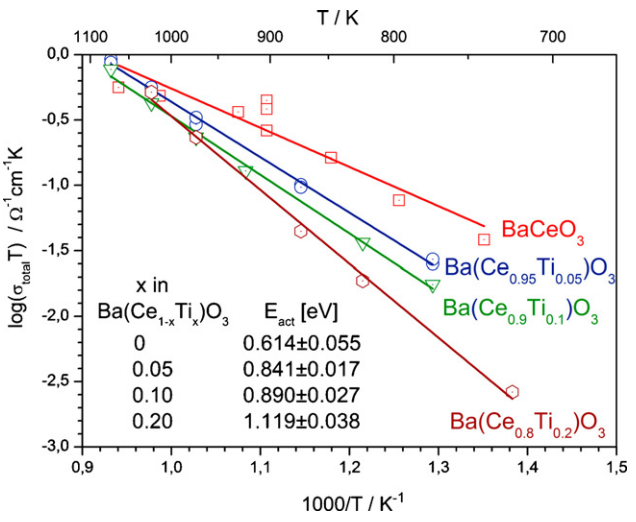

Fig. 6. The dependence of total electrical conductivity on temperature in $\log(\sigma T)$ *vs.* $1/T$ coordinates, for Ti-doped $BaCeO_3$ with different Ti concentrations, compared to undoped $BaCeO_3$ sample.

ing Ce dopant concentration was observed, the opposite effect was anticipated in our case ($BaCeO_3$ doped with Ti).

Fig. 5 shows the dependences of $-\rho''$ on frequency at $T = 500\,^{\circ}C$ for undoped and Ti-doped $BaCeO_3$ as a function of Ti dopant concentration. The increase of Ti concentration leads to the decrease of the maximum frequency, f, which can be attributed to the continuous modification of grain boundary electrical properties with doping.

Fig. 6 shows the dependence of total electrical conductivity on temperature in the Arrhenius coordinates, for the several samples with different Ti concentrations, compared to the undoped sample. In case of Ti-doped samples only total conductivity (controlled by the grain boundary electrical properties) could be determined. For all Ti-doped samples the decrease of total electrical conductivity, comparing to the undoped material, may be observed. This effect is stronger at lower temperatures, where the blocking effect of grain boundaries is extremely dominant. These results are in agreement with the DC conductivity measurements presented previously [8]. The difference in total electrical conductivities determined using DC and EIS methods is caused by the electrode resistance (not added in EIS results).

Current study and the results presented previously [8] clearly indicate that introduction of Ti leads to the drastic decrease of total electrical (and ionic) conductivity of $BaCeO_3$. From the other hand, Ti dopant was used to improve the chemical stability of the mate-

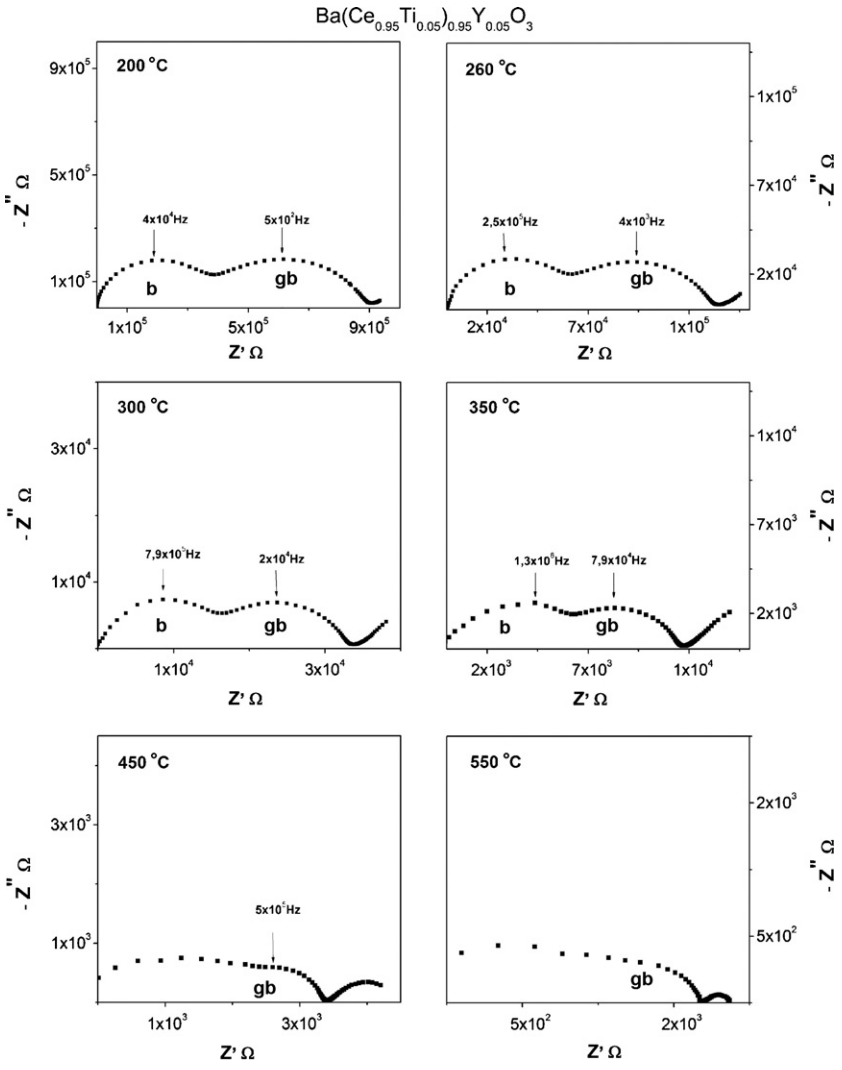

Fig. 7. Example EIS spectra measured for $Ba(Ce_{0.95}Ti_{0.05})_{0.95}Y_{0.05}O_3$ at different temperatures in H_2–Ar atmosphere (7% H_2 in Ar).

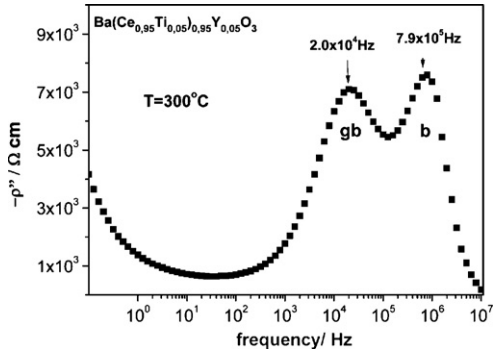

Fig. 8. The dependence of $-\rho''$ *vs.* frequency for $Ba(Ce_{0.95}Ti_{0.05})_{0.95}Y_{0.05}O_3$ sample, at 300 °C.

rial in the presence of CO_2 [12,29]. The optimal properties, namely high electrical conductivity with dominant ionic component and good resistance against the CO_2 may be achieved by the designing the appropriate chemical composition. The introduction of trivalent dopant, e.g. Y^{3+}, to the $BaCe_{1-x}Ti_xO_3$ perovskite structure appeared to be the further logical procedure, as described in Section 1.

The EIS spectra of $Ba(Ce_{0.95}Ti_{0.05})_{0.95}Y_{0.05}O_3$ are shown in Fig. 7. The concentration of Ti ($x = 0.05$) was chosen basing on the results presented in [29]. It was found that the improvement of chemical stability against the corrosion in the CO_2 atmosphere can be reached by Ti doping and the optimal Ti concentration was found to be $x = 0.05$. As can seen in Fig. 7 the impedance spectra are entirely different than that presented in Figs. 1 and 3. Two comparable arcs can be separated straightforwardly for all temperatures.

Fig. 8 shows the dependence of $-\rho''$ on frequency at $T = 300$ °C for $Ba(Ce_{0.95}Ti_{0.05})_{0.95}Y_{0.05}O_3$, determined from the measurements as shown in Fig. 7. Two maxima can be observed for the $f_{gb} = 2.0 \times 10^4$ Hz and $f_b = 7.9 \times 10^5$ Hz, which correspond to the grain boundary and bulk properties, respectively. The comparison of these f_{gb} and f_b values with that obtained for undoped $BaCeO_3$ sample ($f_{gb} = 1.4 \times 10^3$ Hz and $f_b = 1.4 \times 10^6$ Hz) at the same temperature ($T = 300$ °C) indicates that differences in characteristic grain boundary and bulk frequencies, f, were smaller in the case of Ti- and Y-doped sample than in case of undoped sample. The yttrium dopant strongly modifies both grain boundary and bulk electrical properties of the material.

Arrhenius plots shown in Fig. 9 summarize the effect of Y dopant on electrical properties of $Ba(Ce_{0.95}Ti_{0.05})_{0.95}Y_{0.05}O_3$ material. As can be seen, in case of Y-doped material, contrary to both undoped material and Ti-doped material, the grain boundaries are not controlling the total electrical properties of this material. The bulk and grain boundary electrical conductivities are comparable, and the similar activation energies are observed in both cases ($E_b = 0.58 \pm 0.02$ eV, $E_{gb} = 0.64 \pm 0.04$ eV). Moreover, the total electrical conductivity of Y-doped material is higher by ca. one order of magnitude (compared at $T = 500$ °C) than that of Ti-doped materials and similar to undoped material.

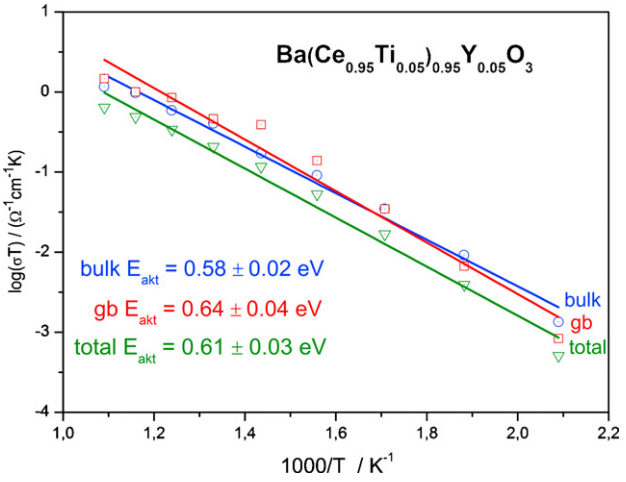

Fig. 9. The influence of Y dopant on bulk, grain boundary and total electrical conductivity of $Ba(Ce_{0.95}Ti_{0.05})_{0.95}Y_{0.05}O_3$ material as a function of temperature, in $\log(\sigma T)$ *vs.* $1/T$ coordinates.

4. Conclusions

The results concerning the influence of Ti and Y dopants on electrical properties determined using the electrochemical impedance spectroscopy measurements as a function of temperature in H_2 containing atmosphere were presented in this paper. The proposed equivalent circuit allowed determination the bulk and grain boundary conductivities and CPE parameters. It was found, that the observed changes of electrical properties caused by the introduction of Ti dopant into the $BaCeO_3$ lattice predominantly results from the modification of the grain boundary properties. The Ti doping caused the substantial decrease of grain boundary electrical conductivity in comparison to undoped material. This blocking effect of grain boundaries was found to be almost independent on the Ti concentration. The total electrical conductivity was controlled by the grain boundary resistivity up to 500–600 °C, whereas at higher temperatures the grain boundary conductivity increased to the level of bulk resistivity. The subsequent introduction of yttrium to the $BaCeO_3$ lattice modified by Ti had the opposite effect. The total electrical conductivity increased, mostly due to the substantial modification of grain boundary electrical properties. The increase of grain boundary conductivity and the decrease of the activation energy indicate that doping with higher concentration of Y may be the effective way in material properties optimization.

Acknowledgement

The financial support of Polish Ministry of Higher Education and Science(MEiN), Project No. K133/T02/2006 (PBZ-KBN-117/T08/103) is acknowledged.

References

[1] H. Iwahara, T. Esaka, H. Uchida, N. Maeda, Solid State Ionics 3–4 (1981) 359–363.
[2] H. Iwahara, H. Uchida, K. Ono, K. Ogaki, J. Electrochem. Soc. 135 (1988) 529–533.
[3] K.D. Kreuer, S. Adams, W. Münch, A. Fuchs, J. Maier, Solid State Ionics 145 (2001) 295–306.
[4] H.L. Tuller, A.S. Nowick, J. Electrochem. Soc. 126 (1979) 209–217.
[5] H. Uchida, N. Maeda, H. Iwahara, Solid State Ionics 11 (1983) 117–124.
[6] G. Ma, H. Matsumoto, H. Iwahara, Solid State Ionics 122 (1999) 237–247.
[7] I. Kosacki, H.L. Tuller, Solid State Ionics 80 (1995) 223–229.
[8] P. Pasierb, E. Drożdż-Cieśla, M. Rekas, J. Power Sources 181 (2008) 17–23.
[9] N. Bonanos, Solid State Ionics 53–56 (1992) 967–974.
[10] M.E. Kompan, Yu.M. Baikov, B.A.-T. Melekh, B.Z. Volchek, Solid State Ionics 162–163 (2003) 1–5.
[11] T. He, K.D. Kreuer, Yu.M. Baikov, J. Maier, Solid State Ionics 95 (1997) 301–308.
[12] A.S. Nowick, Y. Du, Solid State Ionics 77 (1995) 137–146.
[13] H. Iwahara, Solid State Ionics 86–88 (1996) 9–15.
[14] F.L. Chen, O.T. Sørensen, G.Y. Meng, D.K. Peng, J. Eur. Ceram. Soc. 18 (1998) 1389–1395.
[15] M. Oishi, S. Akoshima, K. Yashiro, K. Sato, J. Mizusaki, T. Kawada, Solid State Ionics 179 (2008) 2240–2247.
[16] T. Schober, W. Schilling, H. Wenzl, Solid State Ionics 86–88 (1996) 653–658.
[17] S.-J. Song, E.D. Wachsman, S.E. Dorris, U. Balachandran, Solid State Ionics 149 (2002) 1–10.
[18] K.D. Kreuer, Solid State Ionics 97 (1997) 1–15.
[19] N. Bonanos, Solid State Ionics 145 (2001) 265–274.
[20] G. Ma, T. Shimura, H. Iwahara, Solid State Ionics 110 (1998) 103–110.
[21] K.H. Ryu, S.M. Haile, Solid State Ionics 125 (1999) 355–367.
[22] S.M. Haile, G. Staneff, K.H. Ryu, J. Mater. Sci. 36 (2001) 1149–1160.
[23] S. Wienströer, H.-D. Wiemhöfer, Solid State Ionics 101–103 (1997) 1113–1117.
[24] P. Pasierb, Annales de Chimie-Science de Materiaux 33 (Suppl. 1) (2008) 157–164.

[25] B.-T. Melekh, V.M. Egorov, Yu.M. Baikov, N.F. Kartenko, Yu.N. Filn, M.E. Kompan, I.I. Novak, G.B. Venus, V.B. Kulik, Solid State Ionics 97 (1997) 465–470.
[26] S. Loridant, L. Abello, E. Siebert, G. Lucazeau, Solid State Ionics 78 (1995) 249–258.
[27] Yu Zhi, Ch. Ang, Z. Jing, P.M. Vilarinho, J.L. Baptista, J. Phys.: Condens. Matter 9 (1997) 3081–3088.
[28] D.-Y. Lu, M. Toda, J. Am. Ceram. Soc. 89 (2006) 3112–3123.
[29] P. Pasierb, E. Drożdż-Cieśla, R. Gajerski, S. Łabuś, S. Komornicki, M. Rekas, J. Therm. Anal. Cal., (2009) doi:10.1007/s10973-008-9829-x.